Assessing the Regularity of 3D Triangular Mesh Tessellation Using a Topological Structured Pattern

Naoufel Werghi

Khalifa University, Naoufel.Werghi@kustar.ac.ae

ABSTRACT

This paper presents a new approach for assessing the regularity of a 3D triangular meshed surface. Contrary to other standard methods, our method does not require the computation of any triangle features; it is based exclusively on topological properties, defined at the triangular facet's neighborhood, and exhibits intrinsic scalability. This approach is validated through experiments conducted with a real triangular mesh surfaces. A comparison with standard mesh regularity criteria further confirmed the validity of our method.

Keywords: 3D triangular meshes, mesh regularity assessment, concentric mesh rings.
DOI: 10.3722/cadaps.2011.633-648

1 INTRODUCTION

The last decade has witnessed the proliferation of 3D digitizers, scanners, and substantial developments in techniques for modeling and digitizing 3D shapes. Shape digitalization can be defined as the process of encoding the surface shape into a discrete format suitable for computing purposes such as analysis, visualization, and modelling. Surface tessellation is the backbone of surface digitalization, whereby the surface is encoded by a group of stitched polygons that cover the whole surface. Tessellation can be performed using polygons of any order, but the triangle is the most commonly used. Indeed, triangular mesh is characterised by its simplicity and flexibility; and contrary to other polygons, a triangle is the only polygon in which the vertices are guaranteed to be coplanar. This made the triangular mesh the most supported format in graphics software and hardware. Triangular mesh is used in animation, computer-aided design, simulation training, manufacturing, architecture, and medical and natural sciences, to name just a few. In all these applications, there is always a need to keep the regularity of the mesh tessellation at a reasonable level. Unfortunately, many factors, such as the intrinsic limitations of the 3D scanner, low reflectance of the surfaces, and self-occlusions, can cause missing or deficient data in the digitized surface. At the triangular mesh, this will manifest itself by irregular tessellation, reflected by a large disparity in the triangular facets' features. Therefore, it is necessary to check and assess the regularity of the mesh tessellation in order to ensure the reliability of any subsequent process. This will allow, for instance, for the user to prevent the presence of artifacts in surface visualization, and errors in surface shape analysis and modelling.

Mesh regularity can be perceived as an aspect of mesh quality, but it is not equivalent to it. Indeed, the definition of mesh quality is context-driven and tightly linked to the intended use of the mesh. Contexts include mesh distortion correction [9,12,7,10], mesh optimization and simplification [5,3,6], numerical simulations related to finite element method analysis [8,11 ,1], 3D mesh watermarking [4], and variational tetrahedral meshing [13]. As a matter of fact, a variety of criteria and requirements, for mesh quality, have been defined depending on the application. For example: Faithful approximation to the true surface or the target model, regular and smoothly varying elements, reduced number of elements, and conformity to the boundary regions. Some methods consider that a good mesh is composed of triangles with not too small (needle triangles) and not too large (flat triangles) angles, and thus used the minimum and the maximum angles criteria [7]. Others are based on dimensionless ratios of various geometric parameters [5, 6, 8, and 12]. Another variety of techniques use measures derived from the singular values of a matrix whose columns are formed by the edge vectors of the mesh element [11, 2]. Other methods are based on the distortion amount of the element shape [9, 3, and 10]. In a 3D mesh watermarking context [4], the authors used a metric derived from measures of surface roughness.

2 CONTRIBUTION AND STRUCTURE

We propose a novel approach for assessing the regularity (or homogeneity) of a triangular mesh surface. We consider as an ideal regular mesh the one exhibiting equal-sized triangles, and whereby a mesh composed of equal-sized equilateral triangles represents the perfect instance. Therefore we define the concept of mesh regularity as the extent to which the triangular facets have the same features.
In this work, we propose simple yet effective mechanisms which evaluate the regularity of the mesh triangles. Our approach is distinguished by three characteristics, namely:

1) It is purely based on topological concepts.
2) Does not require the computation of any triangle features.
3) Intrinsically scalable, that is, it can be applied both locally and globally.

However, we point out that the scope of our approach is triangular meshes that are the outcome of a surface digitalization process. It is not meant to deal with CAD mesh models, or mesh surfaces that have been optimized, simplified or manually manipulated.

The rest of the paper will be organised as follows: Section 3 describes the approach, its theoretical foundations and the related algorithms. Section 4 presents the new proposed mesh regularity criterion, and the way it is computed. Section 5 describes the experiments conducted with real digitized surfaces and elaborates on the validation of our approach. Section 6 terminates with a conclusion and potential future work.

3 THE APPROACH

The idea upon which we build our approach was triggered by the observation of an ideal mesh composed of equal-sized triangles. We consider a group of concentric circles on that mesh (Figure 1.a) in which the radii evolve linearly so that the radii of two consecutive circles are r and $r +d$, where d is constant. Given this condition, the number of facets across the rings, defined by successive pairs of circles, is also expected to evolve linearly in the same way, i.e., the number of facets in two consecutive rings will differ by a constant amount. Indeed, we can easily show that the area of a ring ($2\pi rd + \pi d^2$) increases by a constant amount of $2\pi d^2$ from one ring to the next, and therefore so it will be for the number of facets. From this, we can deduce that the number of facets across the rings is expected to follow an arithmetic progression. This condition will not be satisfied for a corrupted mesh (Figure 1.b). Following this reasoning we investigated a mesh regularity criterion based on the progression of the number of triangles across concentric rings, and which can be used as a measure of the mesh regularity at both local and global scale. The design of such criterion demands the

elaboration of a framework for extracting a sequence of concentric rings from an arbitrary mesh. This will be described in the next section.

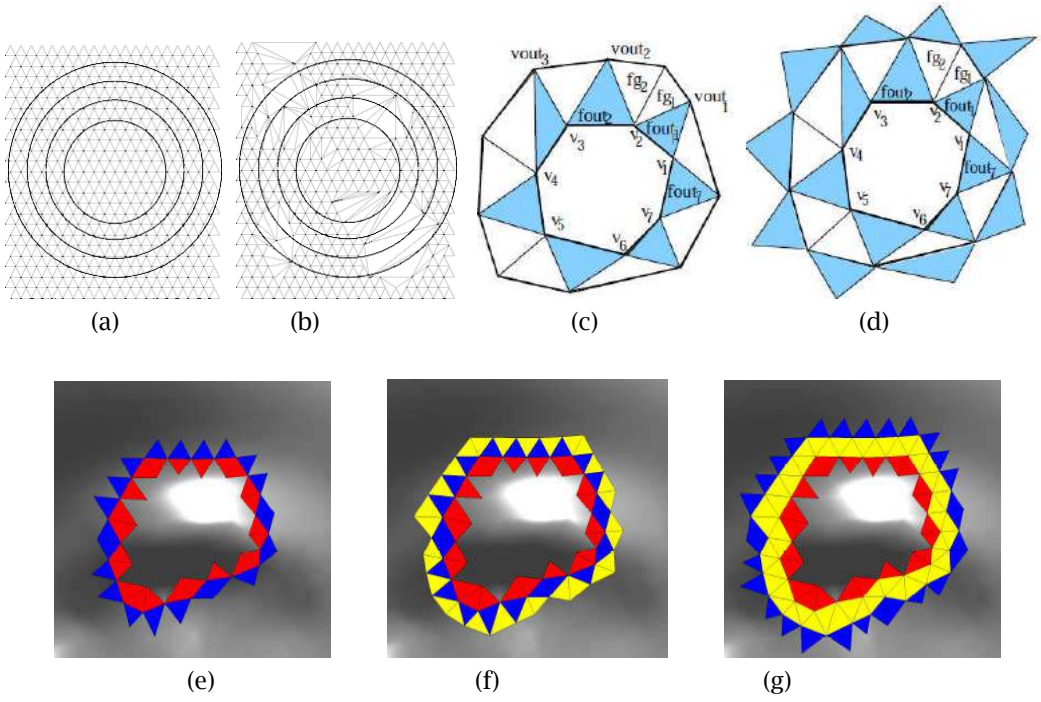

Fig. 1: (a): An ideal mesh composed of equal-sized equilateral triangles. (b): A corrupted mesh. C: *Fout* facets (dark) derived from the contour *E7* (*v_1*, *v_2*, *v_7*). The *Fgap* facets (clear) bridge the gap between pairs of consecutive *Fout* facets. (d): Extraction of the new *Fout* facets. Notice that they are one-to-one adjacent to the *Fgap* facets. (e-f-g): Facet ring construction: (e): The *Fin* and *Fout* facets. (f): Extraction of the Fgap facets. (g): The Fout and the *Fgap* facets are grouped to form the ring, and extraction of the *NewFout* facets that will be used in the construction of the subsequent ring.

3.1 The Facet Ring Concept

By observing the topology of an arbitrary mesh we can notice that the sequence of facets that lie on an inner closed contour of edges (Figure 1.c) can be categorized into two groups, namely, facets having an edge on that contour, and which seem to point outside the area delimited by it. (e.g. *fout_1* and *fout_2* in Figure 1.c), and facets having a vertex on the contour, which seem to point inside the contour's area. Moreover, the facets in the second group look like they are filling the gap between those in the first group (e.g. *fg_1* and *fg_2* in Figure 1.c). Together, the two groups form a kind of ring, which we will conceptualise using the following definitions:

Notation:
i%j: The remainder of the division of *i* by *j*.
En: A piece-wise closed contour composed of n edges, e_1=v_1v_2,…,e_n= v_nv_1.
An: The area bordered by the contour *En*.

Definition 1: *Fout* is a sequence of *n* triangular facets *fout_i, i=1..n*, derived from *En*, such that:

1. *fout_i = [v_i, vout_i, v_((i+1)%n)]* *i=1..n* ;
2. *vout_i* is a vertex outside the area *An* ;
3. *fout_i* ≠ *fout_(i+1)*.

Definition 2: *Fin* is a sequence of *n* facets *fin_i, i=1..n*, one-to-one adjacent to the sequence of *Fout* facets such that:

1. *fin_i = [v_i, vin_i, v_((i+1)%n)), i=1..n*;
2. *vin_i* is inside the area *An*;
3. *fin_i* ≠ fin_(i+1).

Definition 2 implies that facet *fin_i* lies in the area *An* and shares with *fout_i* the edge [v_i, v_((i+1)%n)].

Definition 3: *Fgap_i* is a group of adjacent facets that fill the gap between a pair of consecutive *Fout* facets *(fout_i, fout_(i+1))*. Each *Fgap_i* must satisfy the following constraints:
1) The first facet in *Fgap_i* is adjacent to *fout_i*;
2) The last facet in *Fgap_i* is adjacent to *fout_(i+1);*
3) Each facet in *Fgap_i* contains the vertex shared by (*fout_i, fout_(i+1)*).

We note here that if (*fout_i, fout_*(*i+1*)) are adjacent, then *Fgap_i* is empty.

Definition 4: A facet ring is a group of facets composed of *Fout* facets and their associated *Fgap* facets.

3.2 Facet Ring Construction

Based on the above definitions, we designed a facet ring extraction algorithm dubbed *GetRing*. GetRing processes the *Fout* and *Fin* facets to construct the ring and also to produce new *Fout* facets (Figure 1, d)) to allow for the construction of the subsequent facet ring. Each facet in the new *Fout* must satisfy the constraint of not being part of the constructed facet ring. The procedure *Bridge* described below, retrieve *Fgap_i* facets and their associated *NewFout_i* facets from a pair of *Fout* facets *(fout_i, fout_((i+1)%n))*. *Fgap_i* and *NewFout_i* are one-to-one adjacent. The output *Fgap* encompasses all the *Fgap_i* facets. Figure 1.(e.f.g) depicts an example of a facet ring construction.

Procedure *GetRing*
(Ring, NewFout, Fgap) ← *GetRing(Fout, Fin)*
NewFout ← [ ]; NewFin ← [ ],
For each pair (*fout_i; fout_*(*i*+1)%*n*), *i* = 1..*n*
Append *fout_i* to Ring
(*Fgap_i, NewFout_i*) ← *Bridge*(*fout_i, fin_i, fout_*((*i*+1)%*n*))
Append *Fgap_i* to *Ring*
Append *Fgap_i* to *Fgap*
Append *NewFout_i* to *NewFout*
End for
End GetRing

Procedure Bridge
(*Fg, Fo*) ← Bridge(*f*1*; i*1*; f*2)
(The input and output parameters *Fg, Fo, f1, i1 and f2* are meant to receive Fgap_i, NewFout_i, fout_i, fin_i, and fout_((i+1)%n) respectively.)

if (*f*1*; f*2) are adjacent then
Fg ← [ ]*; Fo* ← [ ]
else
v ← vertex shared by (*f*1, *f*2)

gf ← facet adjacent to *f*1, different from *i*1, and containing *v*
of ← facet adjacent to *gf* and not containing *v*
prev ← *f1*
While (*gf* ≠ *f*2)
append *gf* to *Fg*; append *of* to *Fo*
new_gf ← facet adjacent to *gf*, different from *prev* and containing *v*
new_of ← facet adjacent to *new gf* and not containing *v*
prev ← *gf*;
gf ← *new_gf;*
of ← *new_of;*
End while
End if
End Bridge

The sequence of facets *NewFout_i* returned by the procedure *Bridge* must satisfy the following conditions:

i) Each facet in *NewFout_i* is adjacent to at most one facet in *Fgapi*.

ii) A *NewFout_i* facet does not belong to the ring.

Noticeably, the resulting *NewFout*, which encompasses all the *NewFout_i* facets, inherits the above conditions. However, in an arbitrary mesh, it often happens that the *NewFout* contains pairs of consecutive duplicated facets, reflecting two *Fgap* facets sharing the same adjacent *NewFout* facet (i.e., two out of the three facets adjacent to the *NewFout* facet are *Fgap* facets). To tackle this problem, we apply a filtering procedure that substitutes the duplicated facet with its third adjacent facet (i.e. the one other than two Fgap facets). The condition (ii) is violated when a *NewFout* facet is fused with an *Fgap* facet. Such facets are "trapped" in the facet ring. To fix this anomaly, we apply another round of filtering on the *NewFout* facets to remove these false instances. Figure 2 depicts a violation example of conditions i) and ii) and shows how it is fixed.

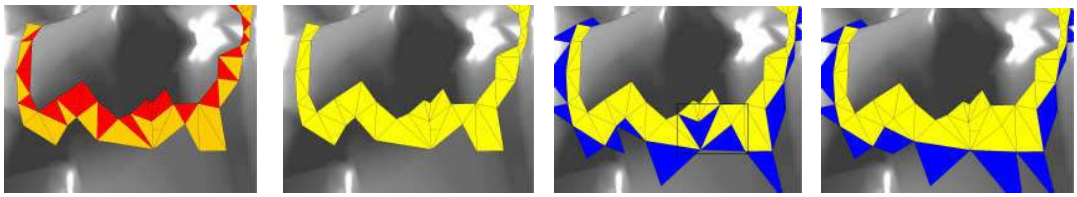

(a) (b) (c) (d)

Fig. 2: (a): The *Fout* facets and their associated *Fgap* facets. (b): The initial constructed ring. (c) Extraction of the *NewFout* facets (dark color). Here we can observe, within the frame, instances of the violation of the conditions i) and ii). The first case is indicated by the *NewFout* facet on the right. This is actually a duplicated *NewFout* facet; if we look back to (a) we will realize that it is adjacent to two *Fgap* facets. The second case is illustrated by the pair of adjacent facets on the left. We can observe that they are located in the ring and not outside as they should be. (d) Fixing the anomalies: The duplicated *NewFout* facet is appended to the ring, and substituted, in the group of *NewFout* facets, by its adjacent facet located outside the ring. The two false instances of *NewFout* facets are simply removed from the group.

3.3 Concentric Rings Construction

By initialising *Fin* and *Fout*, respectively, to a root facet *t* and its three adjacent facets *adj(t),* and by iteratively calling the procedure *GetRing*, we obtain a sequence of concentric rings rooted at the facet

t. For this purpose, we substitute, in *GetRing*, the third output *Fgap* with *NewFin*. This last represents the sequence of facets one-to-one adjacent to *NewFout*, in accordance with definition 2. The *NewFin* is simply derived from the *Fgap* and takes into consideration the outcome of the aforementioned filtering procedures. Hence, the *Fgap* of the i^{th} ring will be the *Fin* of the $(i+1)^{th}$ ring. The corresponding algorithm is as follows:

Procedure ConcentricRings
Rings ← ConcentricRings (*t, adj*(*t*))
    Rings ← [ ]; *Fin* ← *[t, t, t] Fout* ← [adj_1(t), adj_2(t), adj_3(t)]
    For i = 1:*NumberOfRings*
        (*Ring, NewFout, NewFin*) ← *GetRing*(*Fout, Fin*)
        Append *Ring* to *Rings*
        Fout ← *NewFout*
        Fin ← *NewFin*
    End For
End ConcentricRings

4 THE MESH REGULARITY CRITERIA

When applied on an ideal mesh, we can show that the algorithm ConcentricRings produces a sequence of rings in which the number of triangles follows an arithmetic progression of order 12:

$$NbrRingTriangles(n+1) = NbrRingTriangles(n)+12 \quad (1)$$

where *NbrRingTriangles(n)* and *NbrRingTriangles(n + 1)* are the numbers of triangles in the ring *n* and its subsequent *n+1*, respectively. The sequence of the numbers of triangles in ideal n concentric rings is then $\hat{\eta} = [12,24,36,\ldots, 12n]$. Figure 3.a shows an example of three concentric rings in an ideal mesh with a sequence of [12, 24, 36].

This arithmetic progression condition is unlikely to be satisfied in a corrupted mesh, in which the triangles' features exhibit large disparity. We propose the hypothesis that the sequence of the number of triangles across the concentric rings encodes the mesh regularity within the neighborhood formed by these rings. The difference between the ideal sequence $\hat{\eta}_n$ and the computed sequence η_n can be used as metric for evaluating the mesh regularity. Therefore, we propose the following normalized distance as mesh regularity criterion:

$$\Delta_n = \frac{\|\eta_n - \hat{\eta}_n\|}{\hat{\eta}_n} \quad (2)$$

The criterion Δn embeds the extent to which concentric rings are exhibiting a uniform mesh tessellation. Concentric rings having a null Δn (we dub them zero-Δ rings for the rest of the paper) are composed of nearly similar triangles.

Being derived from purely topological concepts, the criterion Δn is invariant to uniform scaling. Figure 3 illustrates an example, in which $\Delta 3$ is computed for a sample mesh patch (Figure 3.b) and colormapped at each triangle. We can observe that $\Delta 3$ keeps the same for the instances of the patch scaled in the x and the y directions (Figure 3.c and 3.d respectively).

Table 1 depicts examples of five concentric rings, extracted from a real mesh surface, and exhibiting tessellation with different degrees of homogeneity. The first sample shows almost equal-sized equilateral triangles, contrary to the last one which contains disparate triangles. We notice that their corresponding sequences (row2) and Δ values (row3) show a clear difference. This primary observation suggests a great potential of the criterion Δ for evaluating the regularity of a triangular mesh.

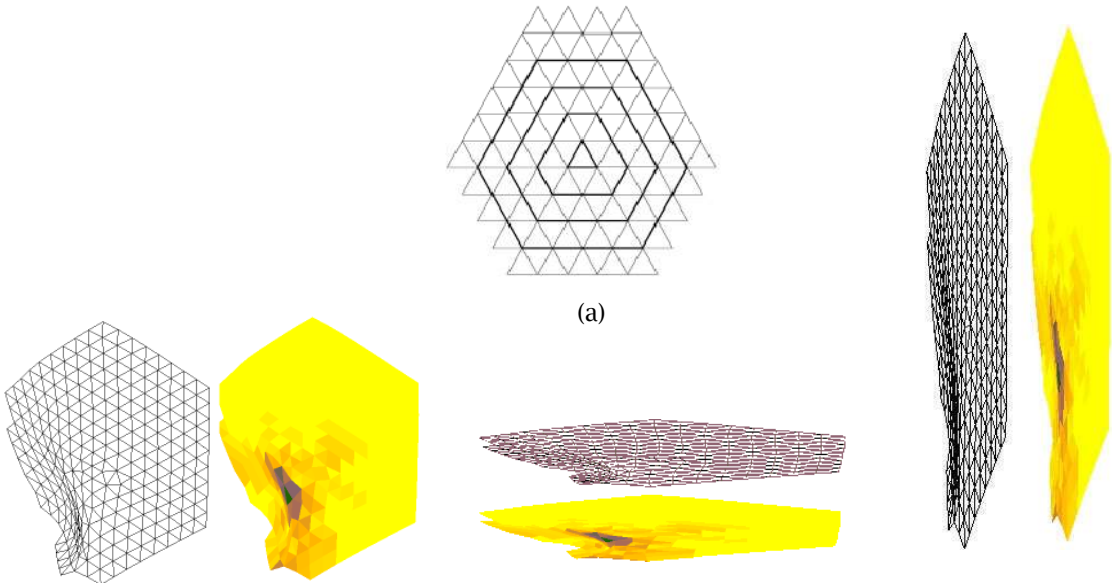

Fig. 3: (a): An example of three concentric rings in regular mesh composed of equilateral triangles. (b) Computation of $\Delta 3$ for a mesh patch. (c) and (d) $\Delta 3$ computed for two scaled instances of the same patch.

Sample	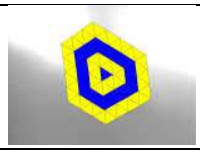	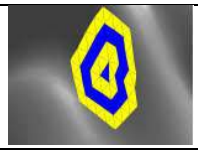	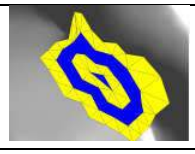	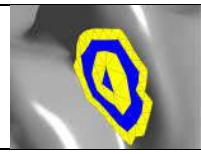	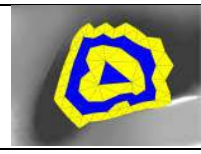
sequence	[12,24,36]	[13,26,38]	[15,30,47]	[16, 38, 49]	[18, 43, 58]
$\Delta 3$	0	0.07	0.28	0.43	0.66

Tab. 1: Samples of concentric rings, their related sequences and $\Delta 3$ error.

5 EXPERIMENTS

We conducted two series of experiments with real mesh surfaces (e.g. acquired via a surface scanning process) and artificial mesh surface models exhibiting different types of tessellations.

5.1 Experiments With Scanned Surfaces

This first series of experiments aims to bring evidence of the following hypothesis: In a real mesh surface :

1. The mesh tessellation in zero-Δ ring areas has a very good regularity.
2. The metric Δ can detect low regularity tessellation areas.

While these two hypotheses look complementary, we deemed that they deserve separate experimentation. For hypothesis 1, one can argue that, in an arbitrary mesh, a zero-Δ rings can exhibit sever irregular tessellation showing low quality triangles (i.e. flat and needle triangles with very large area disparity). While we admit that such configuration is theoretically possible, it is very unlikely

to occur in a mesh that came out from vision-based digitalization. The reason is those light/laser patterns, used in this process, are uniformly projected on the surface. This uniformity will be inherited by the tessellation except at surface regions showing abnormalities, like holes, light saturation, acute curvature etc. This makes the likelihood of the occurrence of the aforementioned case extremely low, at least for a large number of concentric rings, as it will be confirmed in the experiments described in sections 5.1.1 and 5.1.2.

Checking the second hypothesis is motivated by the importance of detecting low regularity tessellation areas in a real mesh, as this allows avoiding erroneous post processing and eventually to perform local mesh correction. Also we did notice that low regularity areas can be used for detecting some features of interest in certain applications (see the comment in the caption of Figure 4). Experiments related to this hypothesis will be described in section 5.1.3

These experiments mentioned above were conducted with triangular mesh surface of a 3D human face scans collected from the BU-3DFE Database [14]. For validation, we employed as ground-truth criteria the following standard triangle parameters:

- The minimum angle in the triangular facet: Min_{angle}.
- The maximum angle in the triangular facet: Max_{angle}.
- The radii ratio regularity criterion : $\rho = R/2r$, where R (respectively r) is the radius of the circumscribed (respectively inscribed) circle.
- The area regularity criterion: $\alpha = \frac{4\sqrt{3}A}{a^2+b^2+c^2}$ where A (respectively a, b, c) is (are) the area (respectively the edges' lengths) of the triangular facet.

ρ and α score 1 for an equilateral triangle. For needle and flat triangles, ρ (respectively α) are largely greater (respectively smaller) than 1.

5.1.1 Experiment 1

In this experiment, we computed the criterion Δ for a 3D mesh face surface samples from the BU-3DFE Database [14]. Facial surfaces in this database exhibit large regular mesh tessellation areas (Figure 4. top). The test performed with these surfaces showed that more than half of the mesh has zero-Δ rings (Figure 4 bottom). This indicates that the mesh is statistically suitable for checking hypothesis 1.

We calculated, for each triangle belonging to a zero-Δ rings in an instance of face mesh surface the parameters Min_{angle}, Max_{angle}, α, and ρ. Then we plotted their histograms in order to examine their distribution. The results are depicted in Figure 5.(a, b, c, d), respectively. We can observe that the majority of the angles are concentrated around 60 degrees, and virtually, the minimum and maximum angles are confined in the intervals [42,60] and [58,90] respectively. These results demonstrate the overall good regularity of the triangles and the quasi-absence of needle or flat angles in the zero-Δ rings. This is further supported by the histograms of α and ρ, where we notice that the concentration of these two criteria is virtually confined in the intervals [0.9,1] and [1,1.5].

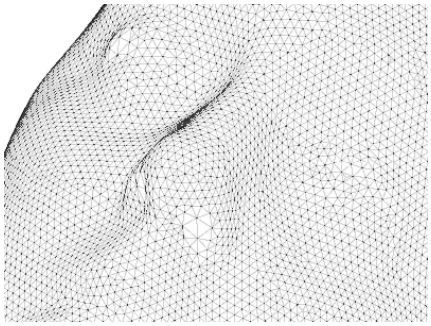
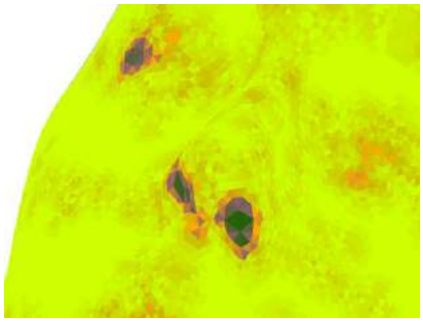

Face	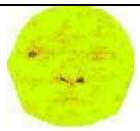				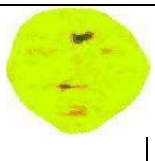	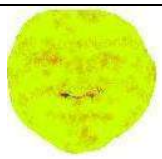
Δ =0 (%)	50	44	49	48	50	46	47

Fig. 4: Top: A sample of a triangular mesh facial surface (left). The color mapping of the error Δ on the mesh (right) shows that large portion of the surface exhibits zero-Δ rings (light color areas). Dark color indicates low regularity tessellation. This is confirmed in the other samples shown in the table, where nearly more than half of the mesh surface encompasses zero-Δ rings. Interestingly, low regularity tessellation areas seem to be located around facial landmarks (nose tip, eyes and lips).

5.1.2 Experiment 2

The results of the first experiment tell us about the overall distribution of the maximum and the minimum angles at the whole set of triangles belonging to zero-Δ rings. However, one can argue that this distribution might not be preserved for each zero-Δ ring, and then some instances might have a large number of flat or needle triangles. To check this, we calculated for each zero-Δ rings, the number of triangles having a Min_{angle} (respectively a Max_{angle}) less than 20^{o} (respectively greater than 160^{o}). The results, depicted in Figure 6.a (Respectively b), shows that almost all the zero-Δ rings have no triangles in these two categories. In the very few that make the exception (5 among 5274, so less than 0.01 %), we notice that four of them only contain two faulty triangles (out of 73: the total number of triangles in three concentric rings), and the other one contains only four faulty triangles. This is a strong indication that in a scanned surface tessellation a null Δ reflects mesh regularity as well as good quality of the triangles within the rings.

In the same vein of the previous experiment, we computed, for each zero-Δ ring, the percentage of facets having a regularity criterion α (respectively ρ) greater than 0.9 (respectively less than 1.1). The related histograms are depicted in Figure 6.c (respectively d). As the histograms indicate, more than 90% of the triangular facets satisfy these conditions. This further confirms the good quality of the triangles and the mesh tessellation in the zero-Δ rings.

5.1.3 Experiment 3

This experiment aims to validate hypothesis 2. That is, the criteria Δ can be used for detecting low regularity tessellation areas. We conducted this experiment as follows: We took the sample face surfaces used in experiments 1 and 2, then we extracted from them all the concentric rings having a large Δ (more than 0.3). Afterwards, we studied the correlation between the criteria Δ and the group of aforementioned standard triangle criteria. Since these criteria are computed triangle-wise, we considered their cumulative sum over the rings as defined below:

$$\beta(t) = \sum_{i=1}^{m} \rho(t_i)$$

$$\lambda(t) = \sum_{i=1}^{m} \alpha(t_i)$$

$$\xi(t) = \sum_{i=1}^{m} Ang_{\min}(t) / Ang_{\max}(t_i)$$

where t (respectively m) is the root facet of (respectively the number of triangles in) the rings. We computed the above criteria for concentric rings containing 2,3,4,5 and 6 rings. As Figure 7(a-e) depict, the plot of Δ together with each of these criteria show clear similarities. This is further confirmed by the Pearson correlation coefficients calculated for the pairs (Δ,β), (Δ,λ) and (Δ,ξ) (Figure 7.f). We notice that for a number of rings up to 4, we obtain correlation coefficients above 0.8. The correlation degrades a little for 5 and 6 rings. However, for the pairs (Δ,β) it keeps remarkably high across all the number of rings.

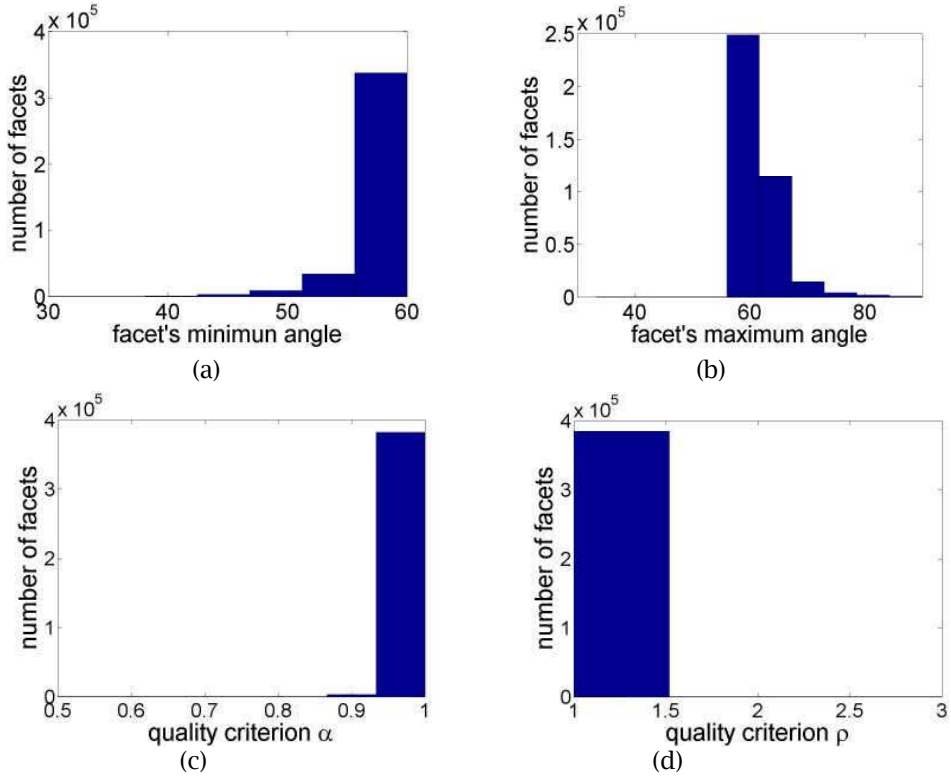

Fig. 5: (a) (respectively (b)): Histogram of the minimal angles (respectively maximal angle) in zero-Δ rings. (c) (respectively (d)): Histogram of the α (respectively ρ) regularity criteria for triangular facets in zero-Δ rings.

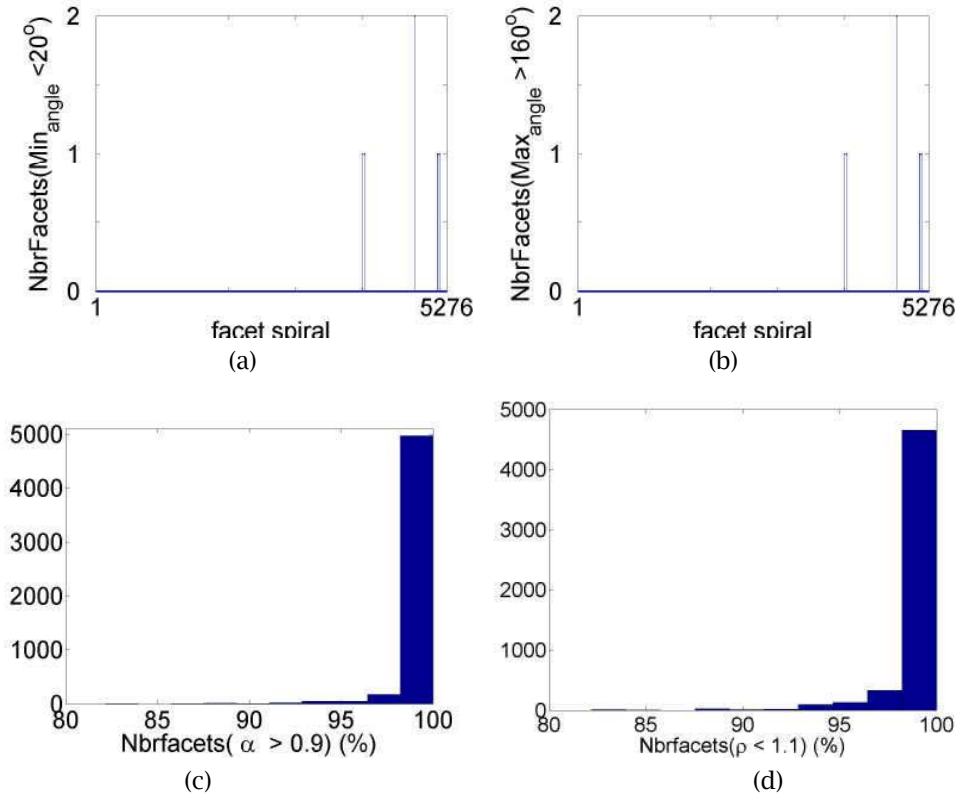

Fig. 6: (a) (respectively (b)): Number of triangular facets in a zero-Δ rings having a minimum angle less than 20° (respectively larger than 160°). (c) (respectively (d)): Histogram of the percentage of triangular facets in a zero-Δ rings having a regularity criterion α (respectively ρ) larger than 0.9 (respectively less than 1.1).

5.2 Experiments With Artificial Mesh Surfaces

The second series of experiments aim to study the behavior of the mesh quality criterion with respect to:

1- Mesh resolution.
2- Varied regular tessellations in the mesh.
3- Random tessellation.

We carried out some tests with synthetic objects generated with MeshLab software [15], and with object models collected from Princeton Shape Benchmark [16], and 3D CAFE repository [17].

In the first test we used a superquadric-like object which surface presents a virtually regular mesh, composed of equal-sized equilateral triangles, except around the singular points (Figure 8.a). We computed the criterion Δ_3 for three instance of the superquadric object having increasing mesh resolution. The results depicted in Figure 8.b shows a similar behavior of the criterion Δ_3 for the different instances, reflecting a clear distinction between zones of regular and irregular tessellations.

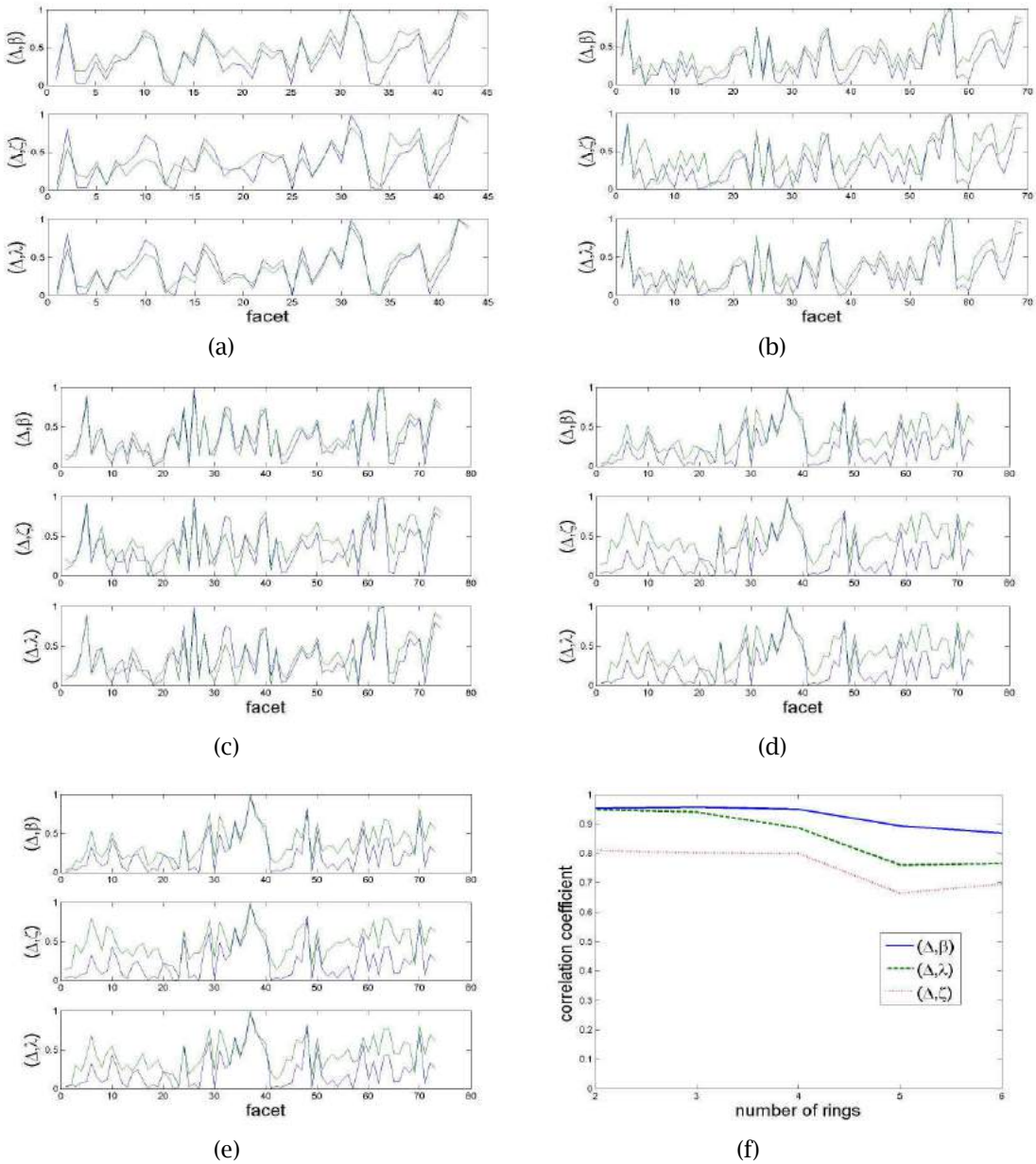

Fig. 7: Plotting of the pairs of criteria (Δ,β), (Δ,ξ), and (Δ,λ) for 2 rings (a), 3 rings (b), 4 rings(c), 5 rings (d) and 6 rings (e). (f): Correlation coefficients between the pairs of criteria for the different numbers of rings.

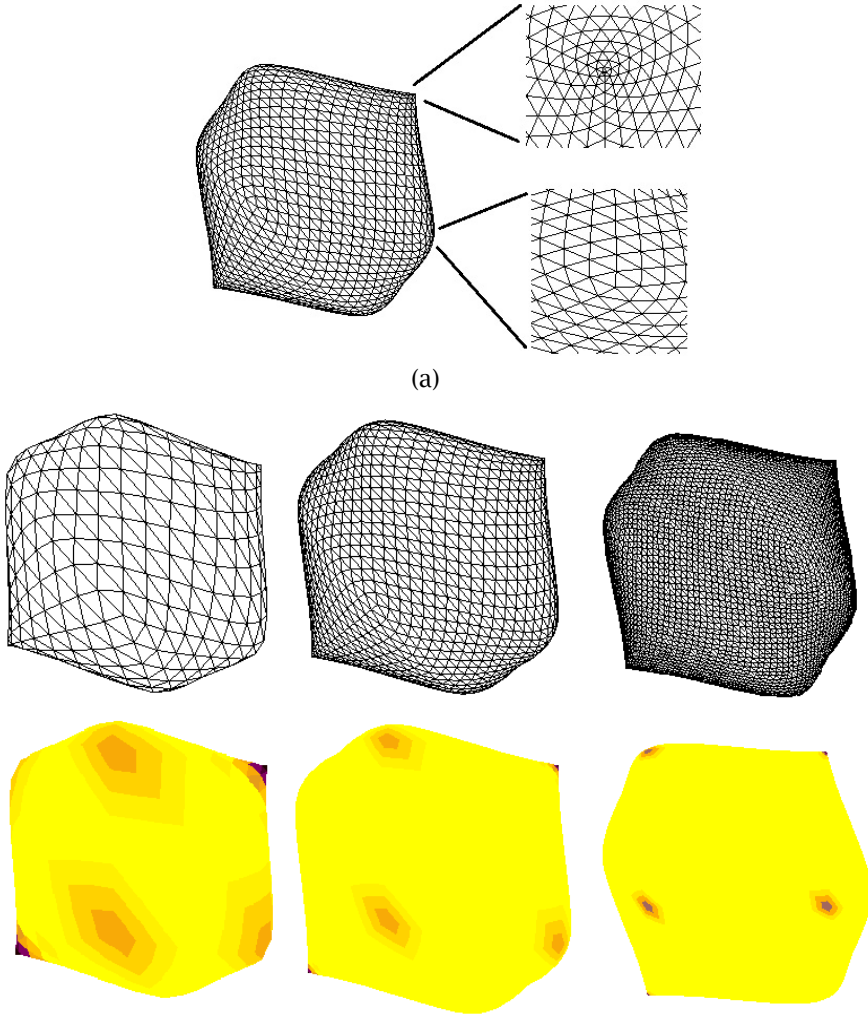

(a)

(b)

Fig. 8: (a): A superquadric object. Virtually, the tessellation is uniform with equal-sized equilateral triangles except at the neighborhood of singular points as shown in the zoomed areas. (b): Computation of the criterion Δ_3 for different mesh resolution.

The second test was carried out with different object models including a sphere, a dodecahedron a cone, and a dinosaur. The objects' surfaces exhibit a kind of region-wise uniform tessellation. In the sphere, nearly all the triangles are equilateral and equal-sized. The tessellation seems uniform across all the surface except at some points where its shows some pattern changes. The dodecahedron and more particularly the cone show different regularly tessellated regions characterized by specific triangle pattern each. As we can see in Figure 9 (bottom), for the three objects, the criterion Δ_3 faithfully reflects the different types of uniform tessellation on the object surface meshes. These results suggest that the criterion Δ can be used as tool for a tessellation-based surface segmentation.

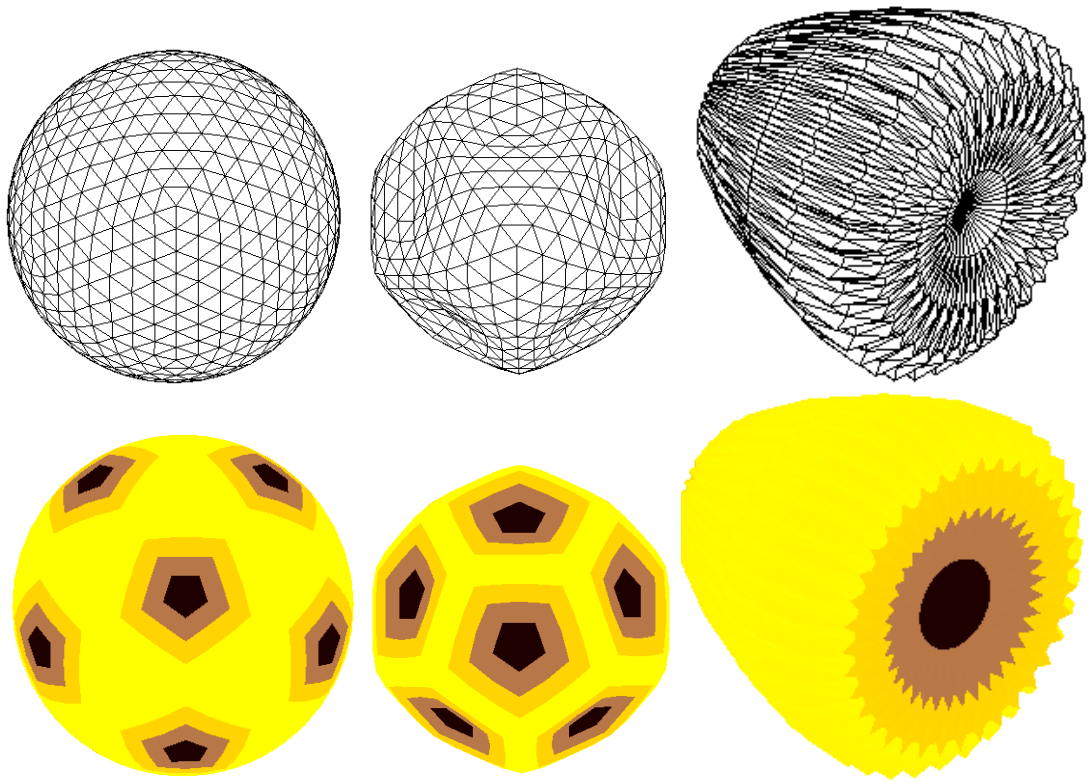

Fig. 9: Examples of mesh models having region-wise uniform tessellation.

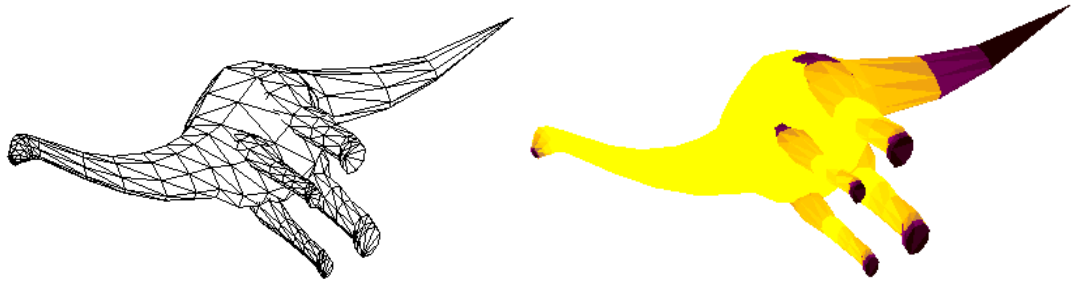

Fig. 10: A dinosaur mesh model and the corresponding $\Delta 3$ computation.

The dinosaur model surface shows also a kind of region-wise regular tessellation (Figure 10). However, contrary to the previous models, the regions exhibit a varying triangle size. We can observe this aspect in the neck and the body tessellation whereby the size of right triangles increases smoothly as we move from the top of the neck down the body. The results show that that $\Delta 3$ looks segmenting the different tessellated regions quite effectively. We notice also the large values that $\Delta 3$ take at the transition areas where the tessellation undergo discontinuities (e.g. at the limbs' extremities).

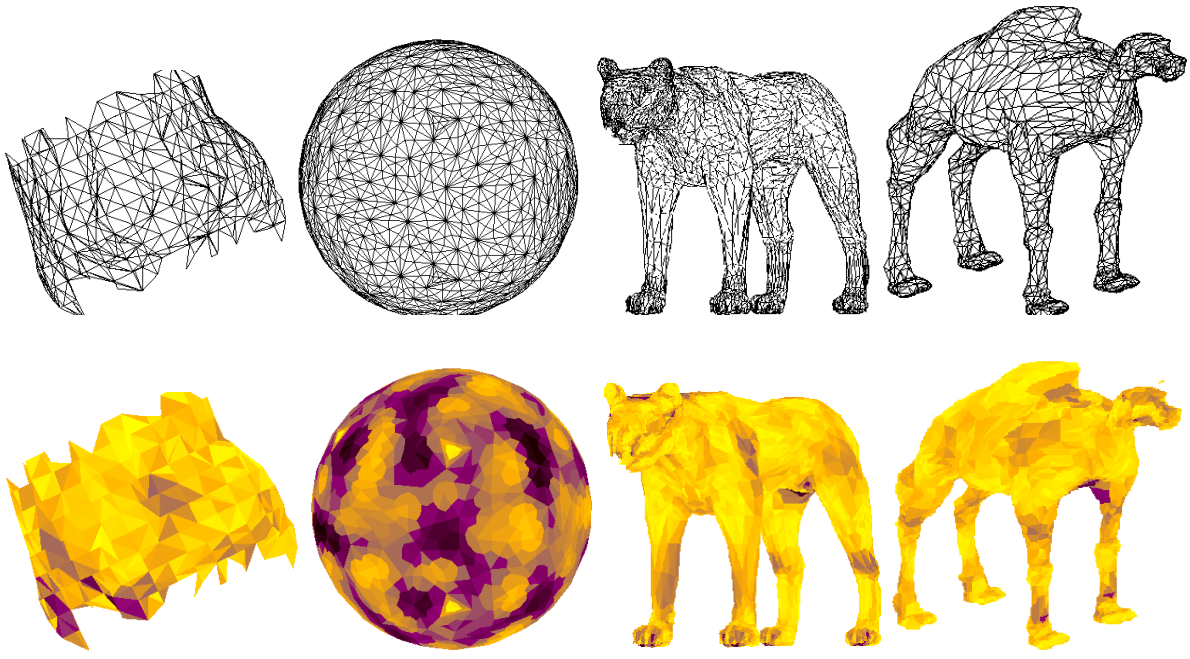

Fig. 11: Objet models with random tessellation and their $\Delta 3$ criteria.

In the last test, we used arbitrary tessellated mesh models including a random shape, a sphere, a panther and a camel (Figure 11). The results clearly show the criterion $\Delta 3$ embeds the randomness of the tessellation across the model surfaces as it is reflected by the randomly colored patches.

These results confirms also that at the individual facet level, the interpretation of a zero-Δ rings in digitized surfaces or artificial mesh like those in Figures 8, 9 and 10, might be different from their counterparts in an arbitrary mesh (like those of Figure 11). In the first category a zero-Δ rings most likely contains similar triangles, but this is not necessarily the case in an arbitrary tessellation. As Figure 11 (bottom) shows, many facets in these randomly tessellated surfaces have a null $\Delta 3$ (the clear colored (yellow) facets) despite the large disparity exhibited by the triangles in their neighborhoods. Therefore, we can conclude that while the criterion Δ can globally inform about the randomness of the tessellation (e.g. by examining its distribution across the whole surface), it cannot be used to detect uniform neighborhoods in an arbitrary mesh.

6 CONCLUSION

In this paper, we presented a novel approach for assessing the regularity of triangular mesh tessellation in a digitized surface. The regularity criterion of our method is based purely on a topological concept. It does not require the computation of any triangle features, such as the angles, edges, or area. The criterion can be employed for an efficient probe of the mesh surface tessellation and fast detection of low regularity tessellation zones. The experiments conducted on a real digitized surfaces and artificial mesh models, showed evidence of the validity of our criterion and its potential for analyzing and segmenting the mesh surface based on the type of the mesh tessellation. Our approach can handle any kind of digitized surface (a surface that went through the normal digitization pipelines). However, it is not meant for optimized mesh surfaces, or CAD model surfaces. In such contexts, the mesh structure is driven by the tradeoff between minimizing the number of triangles and preserving the geometry of the surface. The next issue we plan to explore is how to exploit the

outcome of mesh regularity assessment performed by our criterion in fixing corrupted tessellated areas and enhancing the overall regularity of the mesh. The observation of the outcome of the facial triangular mesh surfaces in Figure 3, suggests investigating the use of our mesh regularity criterion for detecting facial landmarks. While it goes beyond to mesh regularity assessment, we believe that it is an interesting aspect worth to explore in related applications.

REFERENCES

[1] Baker, T.J.: Deformation and quality measures for tetrahedral meshes, Proc. Int. Meshing Roundtable, Albuquerque, NM, U.S.A, 387-396, 2001.

[2] Baker, T.J.: Analysis of triangle quality measures, Mathematics of Computation, 72(244), 2003, 1817–1839. doi:10.1090/S0025-5718-03-01485-6

[3] Canann, S. A.; Tristano, J. R. ; Staten, M. L.: An approach to Combined Laplacian and Optimization-Based Smoothing for Triangular, Quadrilateral, and Quad-Dominant Meshes, Proc. Int, Meshing Roundtable, Dearborn, U.S.A, October, 1998, 479-494.

[4] Corsini, M.; et al.: Watermarked 3D mesh quality assessment, IEEE Transactions on Multimedia, 9(2), 2007, 247-256. doi:10.1109/TMM.2006.886261

[5] Dompierre, J.; et al.: Proposal of Benchmarks for 3D Unstructured Tetrahedral Mesh Optimization , Proc. Int. Meshing Roundtable , Dearborn, U.S.A, October, 1998, 459-478.

[6] Field, D.A.: Qualitative measures for initial meshes , Int. Journal for Numerical Method Engineering, 47, 2000, 887-906. doi:10.1002/(SICI)1097-0207(20000210)47:4<887::AID-NME804>3.0.CO;2-H

[7] Freitag, L. A: On Combining Laplacian and Optimization-Based Mesh Smoothing Techniques, AMD, 220, Trends in Unstructured Mesh Generation, 1997, 37-43.

[8] Frey, P.J.; Borouchaki,H.: Surface mesh quality evaluation, International Journal for Numerical Methods in Engineering. Vol. 45, 1999, 101-118. doi:10.1002/(SICI)1097-0207(19990510)45:1<101::AID-NME582>3.0.CO;2-4

[9] Jacquotte, O. P; Coussement, G.: Structured Mesh Adaptation: Space Accuracy and Interpolation Methods, Computer Methods in Applied Mechanics and Engineering, 101, 1992, 397-432. doi:10.1016/0045-7825(92)90031-E

[10] Kallinderis, Y; Kontzialis,C.: A priori mesh quality estimation via direct relation between truncation error and mesh distortion, Journal of Computational Physics, 28(3) ,2009, 881-902. doi:10.1016/j.jcp.2008.10.023

[11] Knupp, P.: Matrix Norms and the Condition Number, a general framework to improve mesh quality via node-movement, Proc. Int. Meshing Roundtable, South Lake Tahoe, U.S.A., 1999, 13-21.

[12] Parthasarathy, V.T; et al : A comparison of tetrahedral quality measures, Finite Element Analysis and Design, 15, 1993, 255-261. doi:10.1016/0168-874X(94)90033-7

[13] Smit, M.S. ; Bronsvoort, W.F.: Variational Tetrahedral Meshing of Mechanical Models for Finite Element Analysis, Computer-Aided Design and Applications, 5(1-4), 2008, 228-240.

[14] Yin,L; et al.: A 3D facial expression database for facial behavior research, IEEE 7th International Conference on Automatic Face and Gesture Recognition (FG06), Southampton, UK, April 2006, 211-216.

[15] Meshlab software: http://meshlab.sourceforge.net/

[16] Princeton Shape Benchmark, at Princton Shape Retrieval and Analysis Group: http://shape.cs.princeton.edu

[17] 3D CAFE: http://www.3dcafe.com.